metals

Article

Online Prediction of Deformation Resistance for Strip Tandem Cold Rolling Based on Data-Driven

Jianwei Zhao *, Jingdong Li, Haotang Qie, Jian Shao, Xiaochen Wang and Quan Yang

National Engineering Technology Research Center of Flat Rolling Equipment, University of Science and Technology Beijing, Beijing 100083, China
* Correspondence: jianweizhaoustb@163.com

Abstract: An online model is proposed for predicting deformation resistance in the strip tandem cold rolling by combining the back propagation neural network optimized by the mind evolutionary algorithm (MEA-BP) and the deformation resistance analytical model. The real-time collection of hot and cold rolling process data is achieved by constructing a "hot and cold rolling" cross-process data platform. Based on this, a dataset including historical production data of hot and cold rolling is established to train and test the model. The application result of the proposed model shows that the deformation resistance prediction error can be reduced from ±12% to ±5% compared with the traditional analytical model, which demonstrates the model established in this work can effectively improve the prediction accuracy of the deformation resistance in the strip tandem cold rolling.

Keywords: deformation resistance analytical model; mind evolutionary algorithm; BP neural network; deformation resistance prediction

check for updates

Citation: Zhao, J.; Li, J.; Qie, H.; Shao, J.; Wang, X.; Yang, Q. Online Prediction of Deformation Resistance for Strip Tandem Cold Rolling Based on Data-Driven. *Metals* **2023**, *13*, 737. https://doi.org/10.3390/met13040737

Academic Editor: Mohammad Jahazi

Received: 1 March 2023
Revised: 31 March 2023
Accepted: 6 April 2023
Published: 10 April 2023

1. Introduction

With the rapid advancement of society, the market has put forward higher requirements for the quality of cold-rolled strip products, such as external dimensional accuracy, surface quality, and thickness accuracy. However, strip production is a complex industrial system consisting of smelting, continuous casting, hot rolling, cold rolling, and post-treatment processes, which has the characteristics of multiple processes coupled, quality heritability, and nonlinear influencing factors. As shown in Figure 1, the hot rolling line produces strips that become the raw material for cold rolling after heating, high-pressure descaling, rough rolling, finish rolling, laminar cooling, and coiling processes. Due to the radiation, convection, and conduction factors of the hot rolling production process leading to partial heat loss of the strip, the actual finish rolling temperature and actual coiling temperature of each roll of the hot-rolled strip are different, resulting in differences in the mechanical properties of the hot-rolled strip, which has a hereditary effect on the deformation resistance during the cold rolling process. Cai et al. [1] have verified that the finish rolling temperature and coiling temperature have a non-negligible impact on the cold-rolled strip's initial deformation resistance by experiments at different hot rolling temperatures.

Deformation resistance is essential, and its prediction accuracy will directly affect the calculation accuracy of the rolling force and finally affects the control accuracy of quality indexes such as thickness and flatness of cold-rolled strips. The improvement of the strip shape quality of cold rolled finished products depends on the good coordination of several production processes such as hot rolling and cold rolling, as shown in Figure 2. Some efforts have been made to improve the accuracy of deformation resistance. Wang et al. [2] calculated the adaptive learning coefficient of the deformation resistance model using the exponential smoothing method based on the measured data to improve the accuracy of the model. Guo et al. [3] used the Romberg numerical integration approach to calculate deformation resistance before rolling for each stand. Bu et al. [4] developed an online mathematical model for rolling force in the tandem cold rolling process by considering the influence of the deformation zone. However, these studies are based on a single process of cold rolling, which causes a problem of isolation between hot rolling and cold rolling processes and can't fully consider the heritability impact of process parameters of the hot rolling process on the cold rolling process. Thus, the improvement of rolling force prediction accuracy is not very significant for the entire cold rolling process.

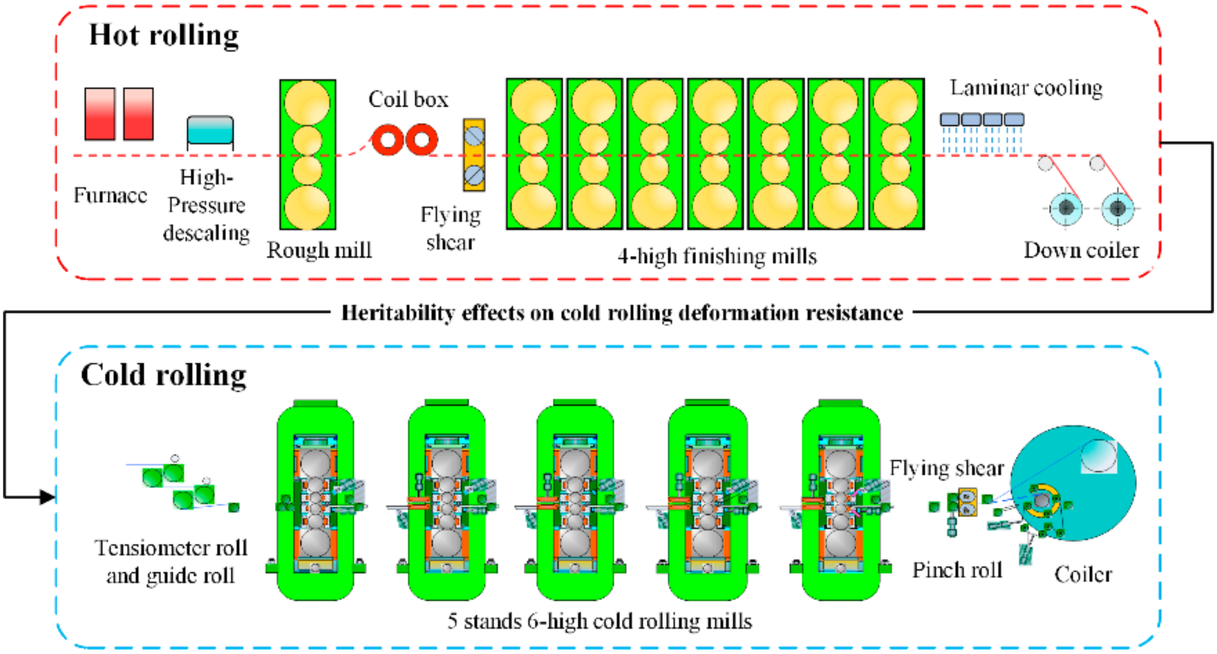

Figure 1. Schematic illustration of hot rolling and cold rolling production process.

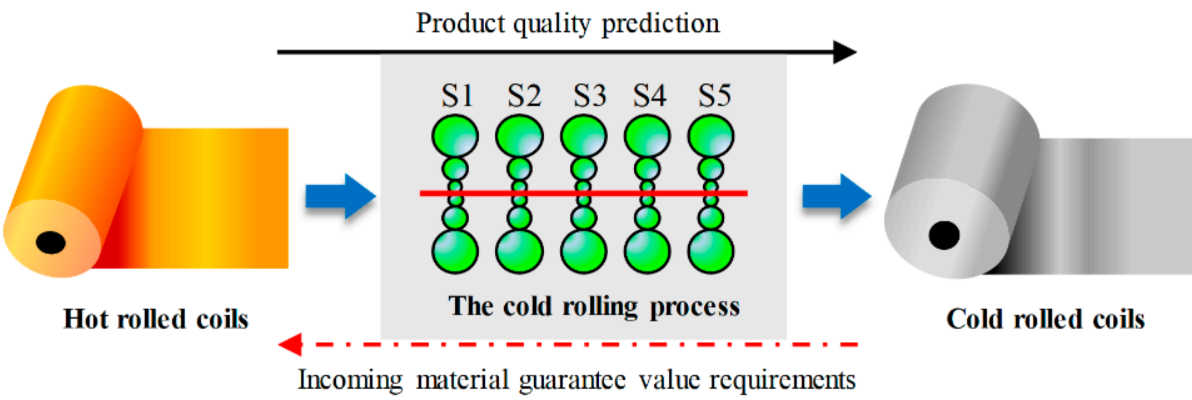

Figure 2. Relationship between incoming material and cold-rolled products.

Since the deformation resistance analytical model cannot consider many nonlinear factors, some scholars have chosen neural network algorithms to help to predict the rolling force. Liu et al. [5] realized the rolling force prediction for a multi-high cold rolling mill by designing a neural network based on a fuzzy cerebellum model. Wu et al. [6] established the rolling simulation model to obtain the sample data and used the simulated sample data to construct a back propagation (BP) neural network for rolling force prediction. Lin et al. [7] combined finite-element and neural network models to achieve the rolling force prediction. Xie et al. [8] established the BP neural network by an adaptive learning algorithm to predict rolling force. Churyumov et al. [9,10] established a model for the steel high-temperature deformation behaviour by an artificial neural network (ANN) and they also achieved the prediction of true stress at hot deformation of high manganese steel by ANN. Jin et al. [11] corrected the strip deformation resistance model by ANN to investigate the load distribution in tandem cold strip rolling process. Wu et al. [12] achieved the deformation resistance prediction of tandem cold rolling by using gray wolf optimization and support vector regression. However, in these studies, none of them avoid the neural network algorithm easily falling into the local optimum. More local extremes may occur when dealing with complex nonlinear problems, which limits the further improvement of model prediction accuracy. Some scholars choose evolutionary algorithms such as genetic algorithms (GA) to optimize the neural network in the rolling field. Zhang et al. [13] used the BP neural network based on GA to predict the deformation resistance and then calculated the rolling force. This method improved the rolling force accuracy compared with the neural network model without the introduction of GA. Sun et al. [14] established an integrated network system by regulating the network's weights using both GA and BP algorithms to predict the rolling forces of a 4-stand tandem cold rolling mill and obtained a good prediction result. However, these studies still don't consider the hot rolling parameters, and ignore the problem that GA's early maturity, slow convergence, and long computation time. Moreover, GA may generate new gene defects during the process of gene mutation. These problems make it difficult to achieve the complete and sufficient optimization of the BP neural network model.

The core of the mind evolution algorithm (MEA) simulates the evolutionary process of human thinking. It not only absorbs the ideas of "group" and "evolution" from the GA but also overcomes the shortcomings of the evolutionary algorithm itself and has fast learning, good adaptability, and a more robust ability to solve nonlinear numerical problems [15,16]. Sun et al. [17] showed experimentally that the MEA's global convergence rate and computational efficiency were improved by more than 20% in nonlinear numerical optimization problems compared to the GA. The studies demonstrate using MEA to optimize neural networks can fully utilize the advantages of both algorithms and improve the performance of neural network models. The data penetration between processes is currently realized, and the feasibility of cold rolling deformation resistance prediction based on the hot rolling process data is available. Therefore, this paper first builds a "hot-cold rolling" cross-process data platform at a rolling industrial site to achieve real-time access to historical production data of hot and cold rolling. Based on obtaining accurate hot rolling data, construct a deformation resistance prediction model by combining the BP neural network optimized by the MEA and the analytical model, given the advantages of the artificial intelligence algorithm and the rigorous theoretical system of the analysis model itself. As shown in Figure 3, the model constructs small networks with the same structure for each stand separately. The actual production data of hot and cold rolling are used for the training of the small network model to make it learn the nonlinear hot, and cold rolling is influencing factors and then make an accurate prediction of deformation resistance for each stand, followed by the completion of the presetting of cold rolling related parameters. Finally, the prediction accuracy and generalization performance of the model are evaluated by historical production data collected by the data platform.

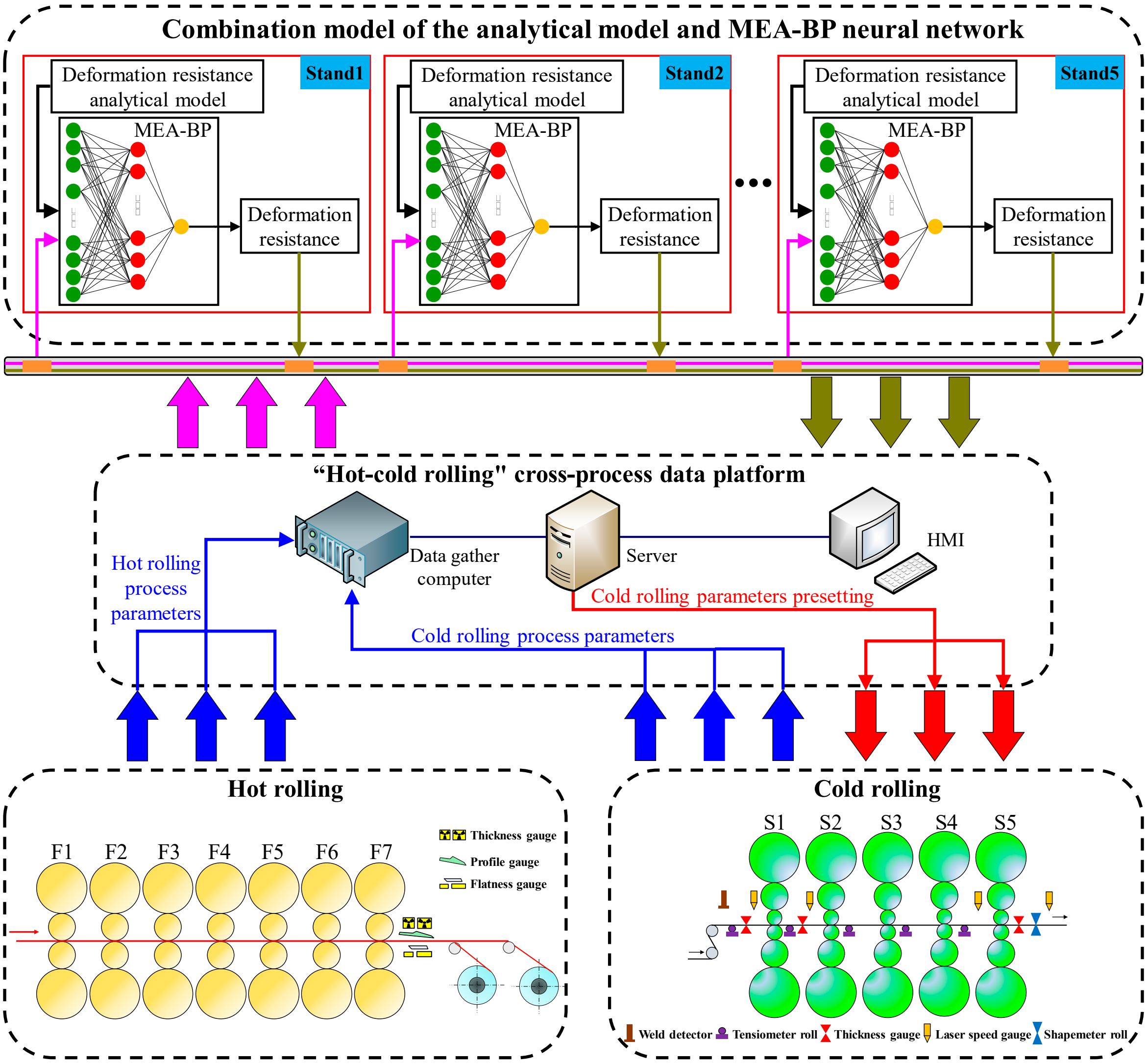

Figure 3. Application of combination model based on "hot-cold rolling" cross-process data platform.

2. Data Acquisition

The quality data of different dimensions of hot rolling mills and cold rolling mills in steel enterprises are scattered in different systems. Cold rolling can currently only obtain the average values of hot rolling process parameters offline. As shown in Figure 4, by building a "hot-cold rolling" cross-process data platform on the industrial site, the cold and hot rolling processes are unified into an organic whole, which enables online real-time acquisition of historical production data of hot rolling and cold rolling, integration of the strip speed-time curve for each process parameter, and then recording the strip sampling data in length coordinates to achieve precise position tracking and removal of abnormal data points in the length direction of the strip, and finally calculating and saving the average value of each critical process parameter corresponding to each roll of the strip as a unit. The dataset is established based on the collected data and the calculation system of the proposed model is deployed on the computing server of the data platform, which can directly call the dataset to train and test the model.

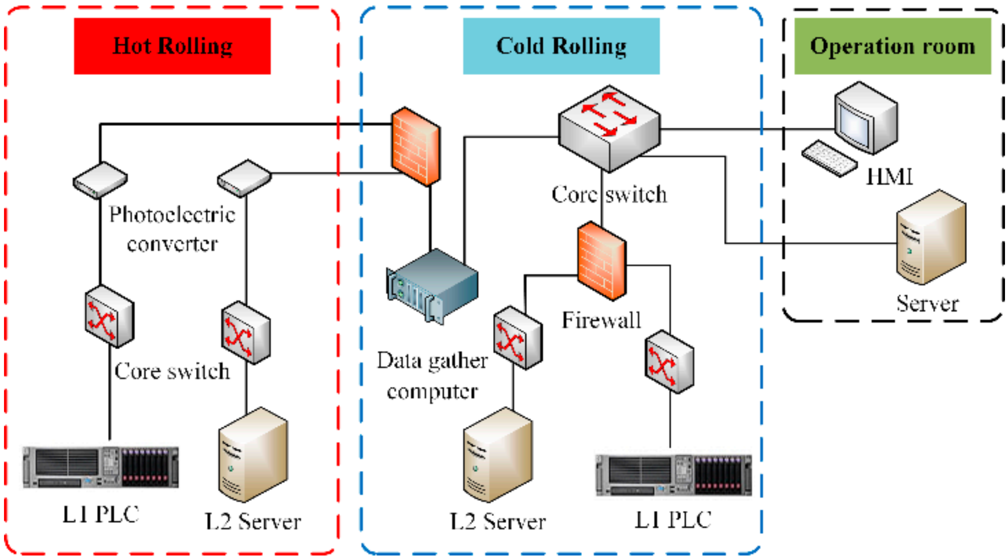

Figure 4. "Hot-cold rolling" cross-process data platform network arrangement diagram.

Instrumentation cannot detect the deformation resistance in the cold rolling process online. In studying the deformation resistance prediction model, accurate deformation resistance is needed as the output of model training and evaluation criteria for optimization. Therefore, in this study, the back-calculation formula of deformation resistance is derived based on the traditional rolling force model. The measured rolling parameters of cold rolling are substituted to back-calculate the calculated value of deformation resistance closer to the actual deformation resistance of each stand. It is called the "actual value" of deformation resistance of cold rolling and the detailed calculation process is as follows.

(1) Traditional rolling force model [18]

$$F = BKK_T Q_P \sqrt{R'(H-h)}, \tag{1}$$

where B is the strip width; K is the deformation resistance; H is the mill entrance strip thickness; h is the mill exit strip thickness. R' is the flattened radius of work roll and can be expressed as:

$$R' = (1 + 2.14 \times 10^{-4} \frac{F}{B(H-h)}) \cdot R, \tag{2}$$

where R is the working roll radius. The tension factor can be calculated by:

$$K_T = (1 - \frac{tb}{K}) \cdot [1.05 + 0.1 \frac{1 - \frac{tf}{K}}{1 - \frac{tb}{K}} - 0.15 \frac{1 - \frac{tb}{K}}{1 - \frac{tf}{K}}], \tag{3}$$

where tf and tb are the forward and backward tensions, respectively. The stress state coefficient is calculated as follows:

$$Q_P = 1.08 - 1.02\varepsilon + 1.79\varepsilon\mu\sqrt{1-\varepsilon}\sqrt{\frac{R'}{h}}, \tag{4}$$

where ε is the relative reduction rate; μ is the friction coefficient, which can be given directly by:

$$\mu = \left(\mu_0 + \frac{\mu_1}{v + \mu_2} + \mu_3 \cdot v\right)\left(\frac{\mu_4}{1 + N_r \cdot \mu_5}\right), \tag{5}$$

where μ_0~μ_5 are the friction coefficient parameters; v is the rolling speed; N_r is the number of steel coils rolled after changing rolls.

(2) Derivation of the back-calculation formula for deformation resistance.

The deformation of Equation (1) yields.

$$KK_T = \frac{F}{BQ_P\sqrt{R'(H-h)}} \tag{6}$$

Let $N_1 = \frac{F}{BQ_P\sqrt{R'(H-h)}}$, and bring Equation (3) into Equation (6) to obtain:

$$K^2 - K(0.75tb + 1.25tf + N_1) - \left(1.05tb \cdot tf + 0.1tf^2 + N_1 tf - 0.15tb^2\right) = 0 \tag{7}$$

The above equation is a quadratic equation with K as the variable, similar to the form $ax^2 + bx + c = 0$. Veda's theorem solves the deformation resistance, and the result is as follows:

$$K = \frac{(\sqrt{N_3{}^2 + 4N_4} - N_3)}{2}, \tag{8}$$

where N_2, N_3, and N_4 are intermediate variables and can be calculated as follows.

$$N_1 = F/\left[BQ_P\sqrt{R'(H-h)}\right] \tag{9}$$

$$N_2 = -(1.05 \times tb + 0.1 \times tf + N_1) \tag{10}$$

$$N_3 = 0.3 \times tb - 1.15 \times tf + N_2 \tag{11}$$

$$N_4 = 0.15 \times tb^2 + N_2 \times tf \tag{12}$$

The main mechanical equipment parameters of the tandem cold mill are shown in Table 1. Relying on the "hot-cold rolling" cross-process data platform, 2848 historical rolling data of strip material MRT-4 are collected. The MRT-4 is the main raw material for tinplate and includes the chemical compositions C, Si, Mn, P, S, N, etc. It is the main product of the application production line, accounting for a large proportion of the overall output. Each cold rolling stand's "actual" deformation resistance values are calculated according to Equation (8), and Figure 5 shows the data distribution for each stand.

Table 1. The main equipment parameters of the tandem cold mill.

Parameter	Stand 1	Stand 2	Stand 3	Stand 4	Stand 5
Work roll diameter (mm)	385~425	385~425	385~425	385~425	385~425
Work roll width (mm)	1420	1420	1420	1420	1420
Intermediate roll diameter (mm)	440~490	440~490	440~490	440~490	440~490
Intermediate roll width (mm)	1410	1410	1410	1410	1410
Back-up roll diameter (mm)	1150~1300	1150~1300	1150~1300	1150~1300	1150~1300
Back-up roll width (mm)	1420	1420	1420	1420	1420
Maximum rolling force (kN)	20,000	20,000	20,000	20,000	20,000
Rated power of motor (kW)	3000	4200	4200	4200	4200
Motor speed (rpm)	300~900	400~1200	400~1200	400~1200	400~1200

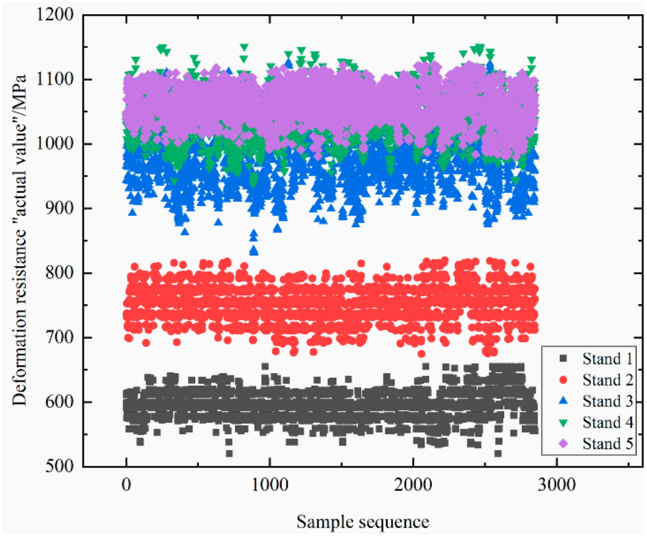

Figure 5. The "actual" deformation resistance distribution of each stand of cold rolling.

3. Modeling

3.1. Analytical Model (AM)

The traditional rolling theory believes that in the whole deformation zone, from the entrance to the exit, the strain rate decreases with the gradual increase of strip deformation until it drops to zero. The combined effect of strain rate and deformation amount makes the deformation resistance constant along the deformation zone, so the deformation resistance of the whole deformation zone can be calculated by the analytical model (AM) with the following formula [19]:

$$K_M = K_S(1000\beta)^{\alpha}, \tag{13}$$

where β is the strain rate; α is a constant; K_S is the static deformation resistance, calculated as follows:

$$K_S = L_a\left(\sum \varepsilon + M_a\right)^{N_a}, \tag{14}$$

where $\sum\varepsilon$ is the accumulated deformation; L_a, M_a, and N_a are empirical coefficients.

A non-linear polynomial regression calculation of L_a and N_a is carried out using the Gaussian Newton method based on the measured parameters, such as the exit and entrance thickness of the strip and the "actual" value of the deformation resistance calculated in Equation (8), which is to achieve self-learning of the deformation resistance analytical model. M_a generally takes a value of 0.01.

3.2. MEA-BP Neural Network

(1) Establishment of BP neural network

BP neural network is a multilayer feed-forward neural network, the features of this network are signal forward transmission and error backpropagation [20]. It is generally believed that a 3-layer BP can approximate any nonlinear surface. Predicting cold rolling deformation resistance is a typical problem of reaching surfaces formed by historical data using neural networks. Figure 6 is the topology of the 3-layer BP and the signal propagation process.

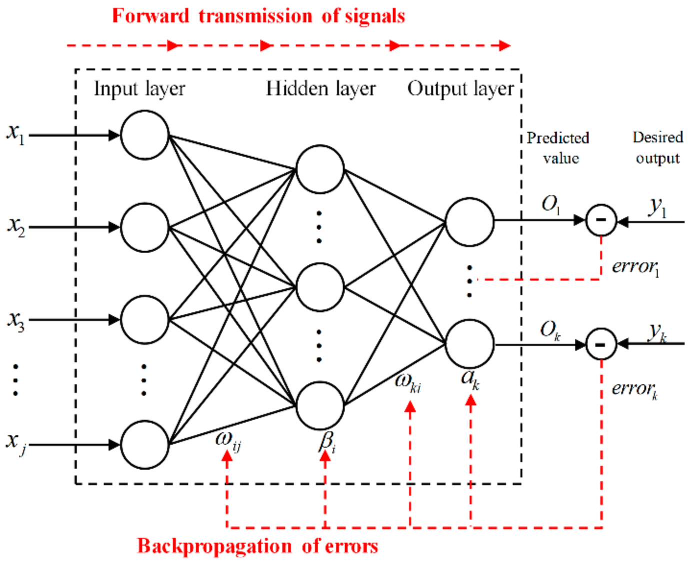

Figure 6. Topology and signal propagation process of BP neural network.

The first step of BP is the forward transmission of the signal. The input value of the network is transmitted from the input layer to the hidden layer through the weighting process, and the hidden layer's output value is acquired after the activation function of the hidden layer is used. The hidden layer's neurons for input and output are calculated as shown in Equations (15) and (16), respectively. The output layer's neurons for input and output are expressed as shown in Equations (17) and (18), respectively [21].

$$net_i = \sum_{j=1}^{q} w_{ij}x_j + \beta_i \tag{15}$$

$$h_i = g(net_i) = g\left(\sum_{j=1}^{q} w_{ij}x_j + \beta_i\right) \tag{16}$$

$$net_k = \sum_{i=1}^{m} w_{ki}h_i + a_k = \sum_{i=1}^{m} w_{ki}g\left(\sum_{j=1}^{q} w_{ij}x_j + \beta_i\right) + a_k \tag{17}$$

$$O_k = f(net_k) = f\left(\sum_{i=1}^{m} w_{ki}g\left(\sum_{j=1}^{q} w_{ij}x_j + \beta_i\right) + a_k\right) \tag{18}$$

where q and m are the numbers of neurons; The weights of the input layer to the hidden layer and the weights of the hidden layer to the output layer are w_{ij} and w_{ki}, respectively. β_i and a_k denote the hidden layer's threshold and the output layer's threshold, respectively. The $g(x)$ and $f(x)$ are the transfer functions in the hidden and output layers, respectively.

For nonlinear problems, the neurons in the hidden layer usually choose nonlinear functions, and the output layer determines linear functions. In this paper, for the highly nonlinear cold rolling deformation resistance prediction, the "Tansig" and "Purelin" functions activate the hidden and output layer, respectively. The formula are as follows:

$$tansig(x) = \frac{2}{1+e^{-2x}} - 1 \tag{19}$$

$$purelin(x) = x \tag{20}$$

The second step is the backpropagation of the error, which begins with the output layer by layer to calculate the output error of each layer neuron, the error will be backpropagated, and layer by layer to correct the connection weights between the layers of the network, so that the error is continuously reduced. Finally, the network's output can be close to the desired value. There are many specific forms of error functions used, and the form of error sum of squares is generally used. The error criterion function E_p for each sample t and the total error criterion function E for T training samples are as follows [22]:

$$E_t = \frac{1}{2}\sum_{n=1}^{k}\left(y_n^t - O_n^t\right)^2 \tag{21}$$

$$E = \frac{1}{T}\sum_{t=1}^{T}E_t = \frac{1}{2T}\sum_{t=1}^{T}\sum_{n=1}^{k}\left(y_n^t - O_n^t\right)^2 \tag{22}$$

where y_n^t and O_n^t represent the desired output and the neural network prediction values, respectively.

(2) The mind evolutionary algorithm optimizes the BP neural network (MEA-BP)

Figure 7 shows the structural framework of MEA, which mainly consists of "Groups", "Subgroups", "Billboard", "Search Environment", and so on. Among them, the global billboard is used to post the information of each subgroup and compare the scores of each subgroup. Individuals within a subgroup post their respective messages and compare scores at a local billboard, performing similar-taxis operations. The score function $M(x)$ is as follows [23]:

$$M(x) = n/\sum_{i=1}^{n}(y_i - O_i)^2 \tag{23}$$

where n is the output neurons number; y_i and O_i represent the desired and predicted output.

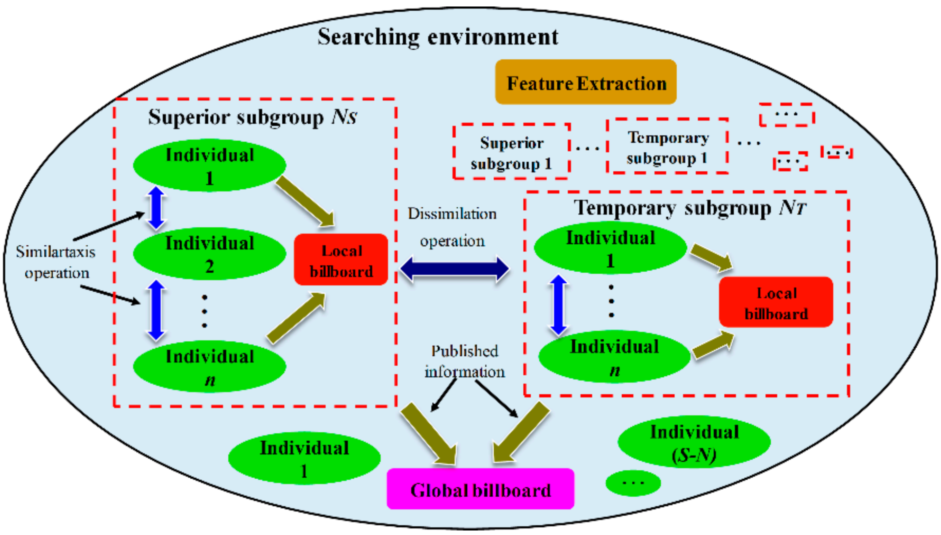

Figure 7. The structural framework of mind evolutionary algorithm.

The core ideas of MEA are as follows.

(1) At the beginning of "learning", S individuals are randomly distributed in the search environment, and N (N = NS + NT) individuals are selected as the initial state by calculating and ranking the scores of each individual. The NS individuals with the highest scores are called the superior individuals, and the NT individuals with high scores are used as temporary individuals. They are used as seeds to form several subgroups divided into superior and temporary subgroups [24]. The feature extraction system analyzes subgroup scores, provides contextual information, and guides the generation of subgroups.

(2) Similar-taxis operation. The process by which individuals compete with each other to become the new superior within all subgroups, with the superior individuals of the subgroup at the center, is called similar-taxis. Until no new superior individual is produced, then the subgroup is said to be mature, the similar-taxis process of the subgroup is finished, and the latest superior individual score is defined as the subgroup score. As shown in Figure 8a,b, most subgroups keep producing new superior individuals, and their scores keep increasing until they finally stabilize, while some other subgroups have no change in their scores because they have not produced new superior individuals.

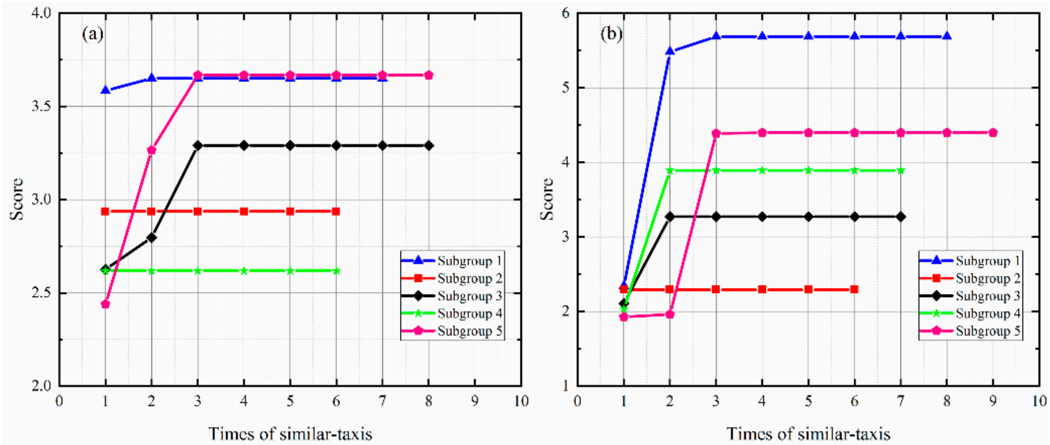

Figure 8. Schematic of similar-taxis operation of subgroups (**a**) superior subgroups (**b**) temporary subgroups.

(3) Dissimilation operation. In the whole search environment, if a temporary subgroup score is higher than that of a mature superior subgroup, the latter is replaced by the former, and the individuals in the original superior subgroup are released; The released individuals have searched globally again and formed a new temporary subgroup to continue steps (2). As the score of subgroup 1 in Figure 8b is higher than that of subgroup 5 in Figure 8a, the former replaces the latter as the new superior subgroup, and the replaced subgroup releases all the individuals who continue to perform the similar-taxis operation. Other subgroups perform the same process. Finally, they are forming a new superior subgroup group and a temporary subgroup group, as shown in Figure 9a,b.

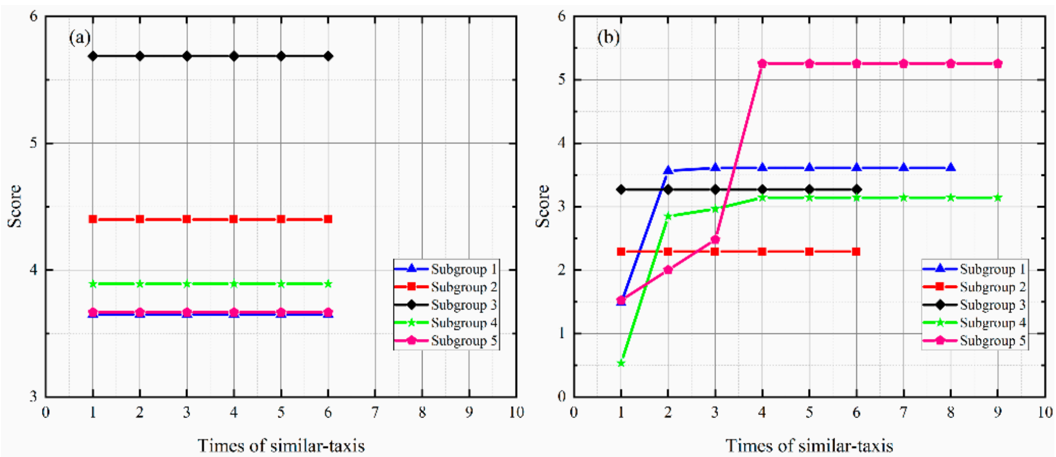

Figure 9. Schematic of similar-taxis operation of subgroups after dissimilation (**a**) superior subgroups (**b**) temporary subgroups.

(4) Repeat steps (2) (3) until met the termination condition.

Based on the above ideas, the flow chart of the MEA-BP is finally determined, as shown in Figure 10, and the processes are as follows.

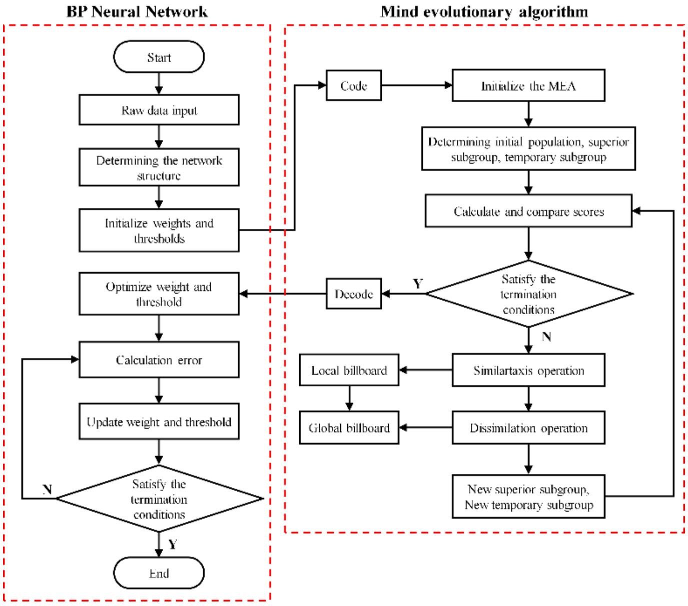

Figure 10. The flow chart of the MEA-BP neural network algorithm.

Step 1: Determine the BP initial parameters. The number of input and output layer neurons is determined by the input and output features of the predicted deformation resistance, respectively. The hidden layer number can be calculated below, where α is a positive integer less than 10.

$$N_{\text{hidden}} = \sqrt{N_{\text{input}} + N_{\text{output}}} + \alpha \tag{24}$$

Step 2: Determine the population size S, the superior subgroup N_S and the temporary subgroup N_T of MEA, randomly generate a certain number of individuals in the environment, and find the superior and temporary individuals according to their scores.

Step 3: Calculate the score. If the termination condition is satisfied, decode these optimal individuals to optimize weights and thresholds into the neural network and start training; if the termination condition is not satisfied, perform similar-taxis operations within each subgroup until the matures.

Step 4: If the subgroup matures, each subgroup score is posted on the global billboard, and the dissimilation operation between the superior and temporary subgroups.

Step 5: Return to Step 3. The optimized weights and thresholds are assigned to train the BP neural network to predict the deformation resistance.

Step 6: When the accuracy of the prediction result meets the termination condition, output the prediction result of deformation resistance for the current stand.

3.3. Combination Model of AM and MEA-BP

(1) Establishment of BP neural network

Firstly, the MEA-BP is constructed based on the metallurgical mechanism to screen the hot and cold rolling process parameters that influence the cold rolling deformation resistance. The magnitude of cold rolling deformation resistance is related to the strain rate and deformation degree and depends on the chemical composition of the metal material. The rolling temperature is constant in the cold rolling process, so the effect of temperature during rolling is ignored. In addition, the deformation resistance is also related to the internal organization state of the metal, trace impurities, etc. Accordingly, it is determined that the input variables of the MEA-BP contain cold-rolled strip entrance thickness, exit thickness, relative reduction rate, cumulative reduction rate, rolling speed, and the hot rolling process parameters that have the most significant influence on the deformation resistance in the upstream hot rolling process, finish rolling temperature, coiling temperature, and finished slab thickness.

Secondly, because of the rigorous theoretical system and physical significance of the analytical model of deformation resistance, the calculated value of the AM is directly used as an input item of MEA-BP to establish a combination model without destroying the self-learning process of the deformation resistance analytical model. As shown in Figure 11, the MEA-BP deformation resistance prediction model has been constructed for each stand, so that the accurate prediction of the deformation resistance of the five stands in the strip tandem cold rolling can be achieved. Figure 12 shows the network structure of single stand. Each small network input term includes the process parameters of hot and cold rolling in Table 2 and outputs a predicted value of deformation resistance of the current stand. Since modeling by steel grade, not consider the influence of chemical composition. Finally, building the above neural network model by using Python language under Windows system.

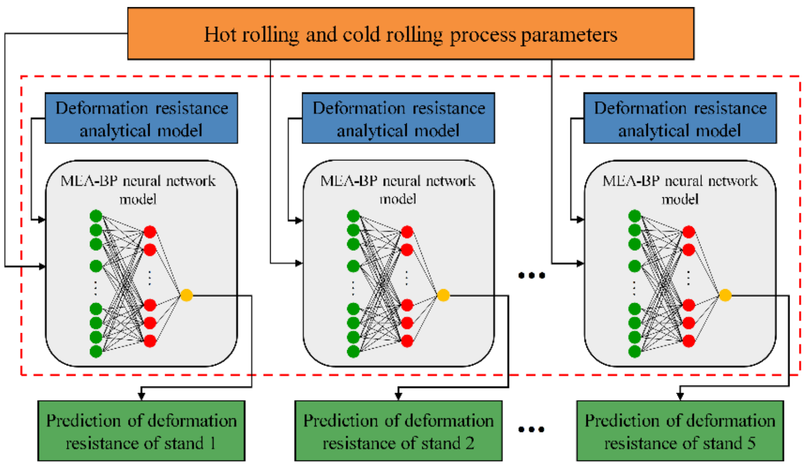

Figure 11. The main structure of the deformation resistance prediction model.

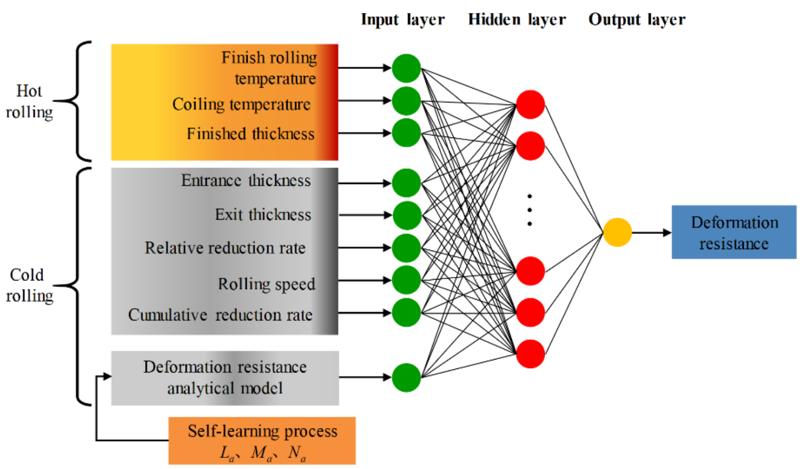

Figure 12. Schematic illustration of the neural network structure for a single stand.

Table 2. Descriptive statistics of the input parameters.

No.	Symbol	Physical Interpretation	Range	Unit
1	H	Entrance thickness	0.29~2.29	mm
2	h	Exit thickness	0.19~1.41	mm
3	ε	Relative reduction rate	0.25~0.45	-
4	ζ	Cumulative reduction rate	0.35~0.89	-
5	v	Rolling speed	156~1627	m/min
6	FDT	Finish rolling temperature	846~882	°C
7	CT	Coiling temperature	555~580	°C
8	H_0	Hot rolling finished thickness	1.89~2.29	mm
9	KM	Deformation resistance analytical model	710~1081	MPa

4. Results and Discussions

Firstly, to verify the merits of AM and MEA-BP for cold rolling deformation resistance prediction, the combination model in this study is named MEA-BP-AM. The MEA-BP, GA-BP, and BP neural network models were also selected, and parameters 1~8 in Table 2 were used as input terms of the models to participate in the comparison tests, MEA-BP GA-BP, and BP, respectively. Section 4.2 presents the prediction results of the AM, GA-BP, BP, and MEA-BP-AM for deformation resistance, and Section 4.3 presents the performance evaluation results of the BP, GA-BP, MEA-BP, and MEA-BP-AM models. Secondly, comparative test models are set up in this study to explore the effect of hot rolling process parameters on cold rolling deformation resistance. The same four models mentioned above are selected. Only the 1st to 6th cold rolling process parameters described in Table 2 are involved in the comparative test as inputs to the models. The performance evaluation results of the models are presented in Section 4.3.

4.1. Execution of Model

The 2848 hot and cold rolling data of the same steel grade described in Section 2 were used for the accuracy testing of the model. Since most of the process parameters in the actual rolling process are measured by sensors and the quality of the acquired data is poor, to improve the essential prediction capability of the model in the field, this study removes the incorrect data points from the measured data using the 3σ confidence interval criterion.

After data cleaning, the remaining representative data were 2670, of which 70% were selected as the training set and 30% as the prediction set. Then, the data are normalized to remove the influence of units between different data and turn them into a dimensionless data set. In this paper, the Max-Min normalization method is used to transform and deform the original data using linear transformation processing to form a data set with a value domain of [0, 1], as follows, where x is the original data; $x_{\max}$ is the maximum value in the original data; $x_{\min}$ is the minimum value in the original data; x_N is the normalized data.

$$x_N = \frac{x - x_{\min}}{x_{\max} - x_{\min}} \tag{25}$$

The parameters used in the model were finalized through several experiments, and the specific values are shown in Table 3. Where γ is the learning rate, c is the convergence error, S is the population size, i is the maximum number of iterations, Pm is the probability of variation, P_c is the crossover probability, N_T is the number of temporary subgroups, and N_S is the number of superior subgroups.

To evaluate each model's prediction accuracy and generalization ability, the mean absolute error (MAE), mean absolute percentage error ($MAPE$), and root mean squared error ($RMSE$) are employed as the performance criteria [25]:

$$MAE = \frac{1}{n}\sum_{i=1}^{n}|y_i - O_i| \tag{26}$$

$$MAPE = \frac{1}{n}\sum_{i=1}^{n}\left|\frac{y_i - O_i}{y_i}\right| \times 100\% \quad (27)$$

$$RMSE = \sqrt{\frac{1}{n}\sum_{i=1}^{n}(y_i - O_i)^2} \quad (28)$$

where y_i and O_i are the test set's desired output and prediction values, respectively.

Table 3. Parameter settings of different models.

Model	Parameter and Value
BP	c = 0.001; γ = 0.01
GA-BP	c = 0.001; γ = 0.01; S = 40; Pm = 0.05; Pc = 0.07; i = 50
MEA-BP, MEA-BP-AM	c = 0.001; γ = 0.01; S = 100; N_S = 5; NT = 5; i = 50

4.2. Prediction Results

Figure 13a–d shows the prediction results of AM, BP, GA-BP, and MEA-BP-AM models for the test set. As shown in Figure 13a, the error distribution of the deformation resistance calculated using the AM is ±12%, and the linearity between the computed results and the actual deformation resistance is poor. As shown in Figure 13b,c, the errors of the predicted deformation resistance using the BP and the GA-BP were distributed at ±10% and ±8%, respectively, and the optimization of the BP neural network by GA improved the prediction accuracy the BP for cold rolling deformation resistance. As shown in Figure 13d, the error of the prediction results of cold rolling deformation resistance by MEA-BP-AM is reduced to within ±5%. The combination of the AM and MEA-BP gives full play to the advantages of both. It improves the prediction accuracy of cold rolling deformation resistance by the analytical and artificial intelligence models alone.

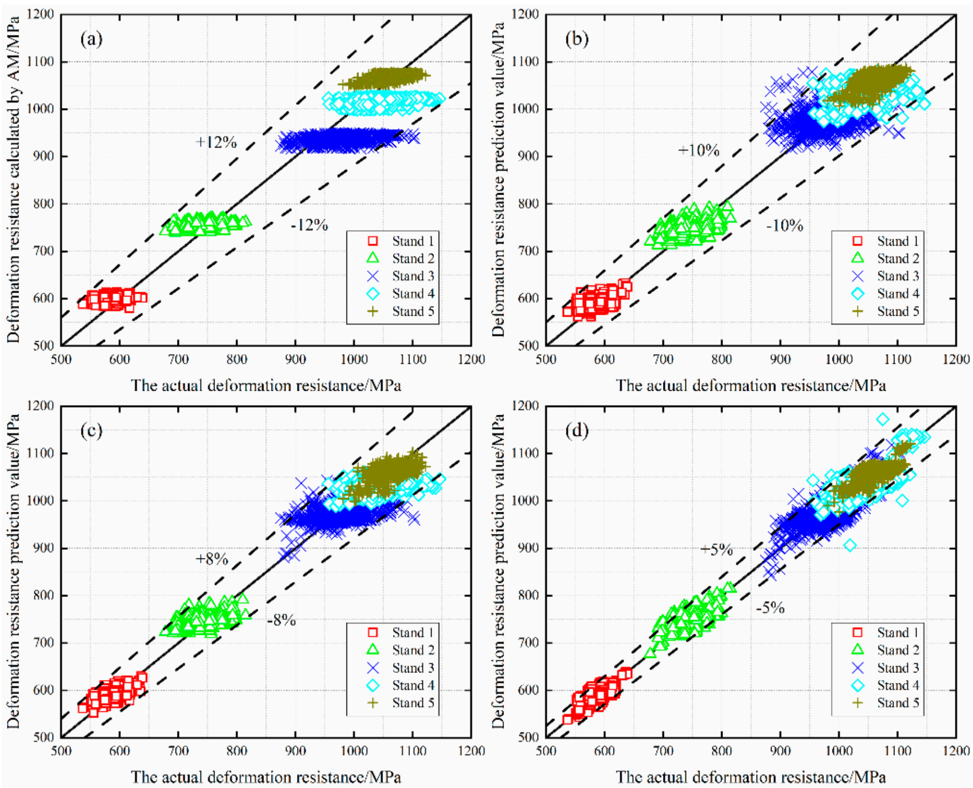

Figure 13. Calculation results of the deformation resistance (**a**) AM (**b**) BP (**c**) GA-BP (**d**) MEA-BP-AM.

In addition to this, the reasonableness of the distribution of deformation resistance prediction errors is also a measure of the performance of the deformation resistance prediction model. Figure 14 shows the relative error distribution between the deformation resistance predicted for each stand using the MEA-BP-AM model and the actual deformation resistance of each stand. As can be seen in Figure 14, the histogram of the relative error distribution of deformation resistance for any of the five cold-rolled stands is more stable, with the fitted curve showing the shape of a normal distribution centered on 0, low on either side, and high in the middle, and approximately symmetrical, with a better overall performance.

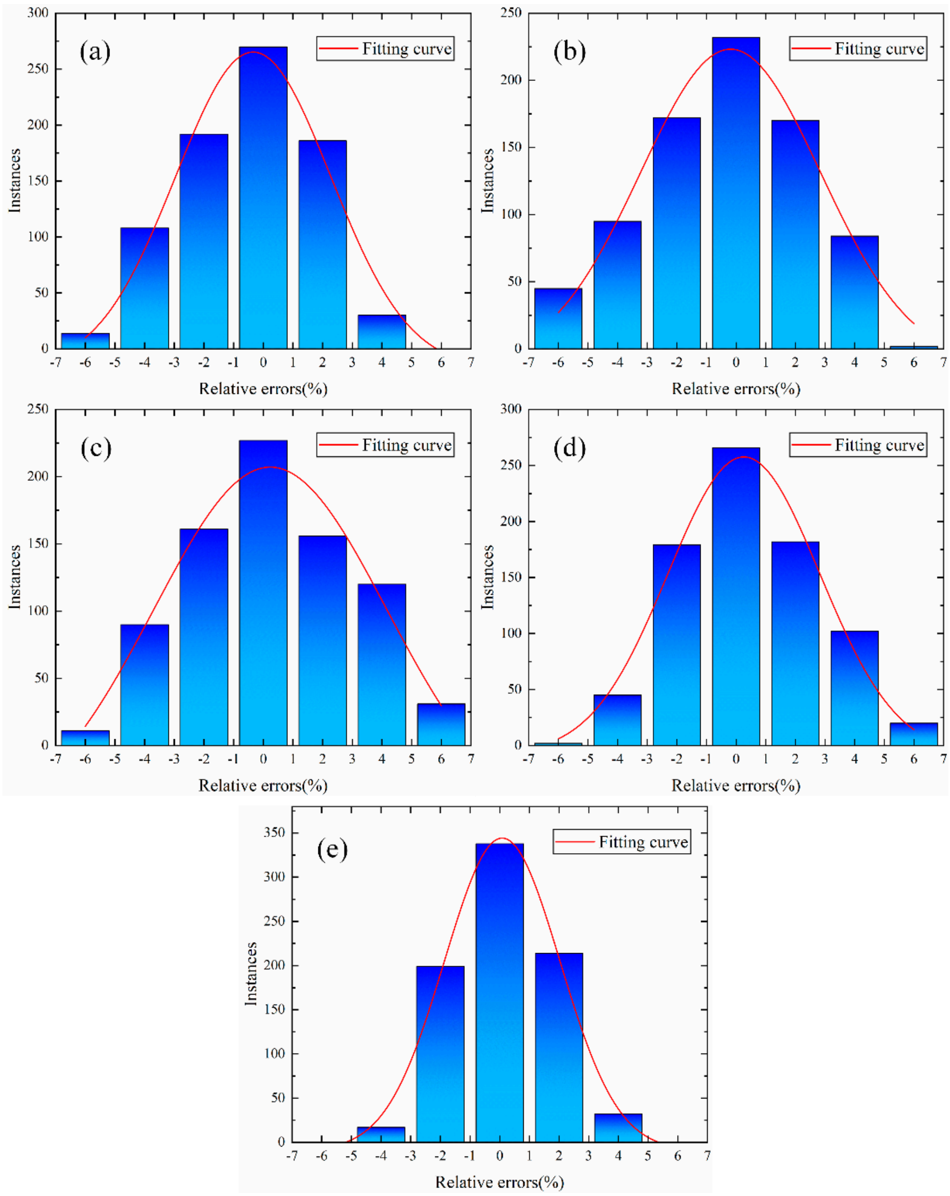

Figure 14. The relative error between predicted and actual values of deformation resistance of the MEA-BP-AM model. (**a**) Stand 1 (**b**) Stand 2 (**c**) Stand 3 (**d**) Stand 4 (**e**) Stand 5.

4.3. Performance Criteria

Tables 4 and 5 show the results of the model performance evaluation considering and not considering the hot rolling process parameters as input, respectively, where all the results are averaged over 30 experiments performed on the test set to avoid the effect of chance errors. Best performance bolded. It is found that the model prediction capability for deformation resistance is improved to different degrees, and the prediction error is smaller when considering the hot rolling parameters as inputs to the model compared to relying on the single process modeling of cold rolling. By looking at Table 4, it can be found that the MEA-BP-AM model outperforms the MEA-BP, GA-BP, and BP in all aspects. Meanwhile, after optimizing the BP neural network using GA or MEA, both improved the prediction performance of the BP to different degrees and reduced the prediction error. Still, the model version optimized by using MEA for the BP neural network was better. The prediction accuracy was higher for the MEA-BP than the GA-BP, also reflected in Table 5. Figure 15 visualizes the effect of the hot rolling parameters on the predictive performance of the MEA-BP-AM model when used as input to the model. As seen in Figure 15a–e, the prediction error of the MEA-BP-AM model is reduced, and its performance is improved when the hot rolling parameters are considered as inputs to the model. The effect of the hot rolling parameters on the cold rolling deformation resistance is not negligible.

Table 4. Performance of models considering hot rolling parameters.

Stand	BP			GA-BP			MEA-BP			MEA-BP-AM		
	MAE	MAPE (%)	RMSE	MAE	MAPE (%)	RMSE	MAE	MAPE (%)	RMSE	MAE	MAPE (%)	RMSE
1	12.49	2.13	15.39	11.79	2.01	14.35	11.53	1.96	14.03	11.06	1.88	13.41
2	17.35	2.34	21.47	17.18	2.32	21.21	16.97	2.29	21.00	15.92	2.15	19.60
3	31.07	3.18	40.65	29.06	2.97	37.67	28.32	2.89	35.95	25.40	2.59	32.09
4	23.99	2.28	31.56	23.33	2.21	30.84	22.26	2.12	28.59	20.24	1.93	25.84
5	16.59	1.56	19.92	16.11	1.51	19.92	15.70	1.48	18.86	14.71	1.38	17.99

Table 5. Performance of model without considering hot rolling parameters.

Stand	BP			GA-BP			MEA-BP			MEA-BP-AM		
	MAE	MAPE (%)	RMSE	MAE	MAPE (%)	RMSE	MAE	MAPE (%)	RMSE	MAE	MAPE (%)	RMSE
1	13.73	2.34	16.83	**12.90**	**2.19**	15.78	13.29	2.26	16.18	12.92	2.19	15.48
2	18.73	2.54	23.26	18.62	2.52	23.34	18.15	2.46	22.41	17.48	2.36	21.23
3	31.74	3.26	43.17	31.85	3.26	42.73	30.30	3.09	38.61	27.64	2.84	34.39
4	25.03	2.37	32.50	23.20	2.22	30.58	22.67	2.15	29.77	21.50	2.04	28.00
5	17.41	1.64	20.93	17.26	1.62	20.75	16.81	1.58	20.19	16.44	1.54	19.74

4.4. Field Test

To further verify the accuracy and performance of the proposed model, the values of deformation resistance predicted by the traditional AM model and the proposed MEA-BP-AM model are adopted in the rolling force setting model of a 1420 mm strip cold rolling line, respectively. Since the prediction accuracy of rolling force only depends on the value of deformation resistance when other parameters are consistent, the relative errors between the predicted and measured rolling forces for different stands are employed to evaluate the prediction accuracy of deformation resistance. The comparison of relative errors of rolling force between two models for different stands is shown in Figure 16. Overall, the relative errors of rolling force based on the MEA-BP-AM model are smaller than that based on the AM model for each stand. Compared with the traditional AM model, the average relative error of rolling force decreases from 6.1% to 4.3% in stand 1, from 3.9% to 3.2% in stand 2, from 7.6% to 6.4% in stand 4, and from 5.6% to 4.5% in stand 5 after using the proposed MEA-BP-AM model. It can be seen that the rolling force accuracy of each stand has been improved to varying degrees.

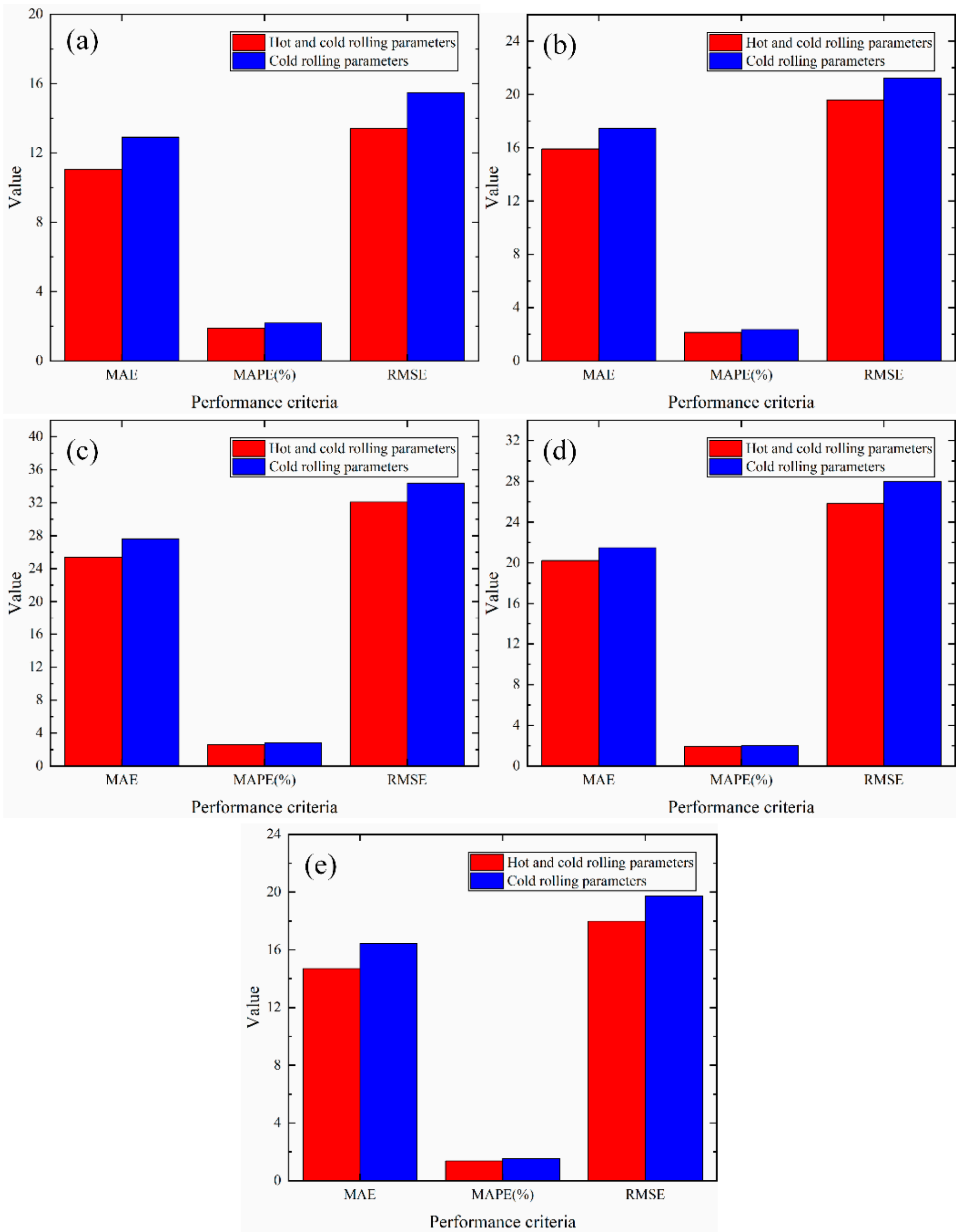

Figure 15. Error histogram comparisons of MEA-BP-AM models for without considering hot rolling parameters. (**a**) Stand 1 (**b**) Stand 2 (**c**) Stand 3 (**d**) Stand 4 (**e**) Stand 5.

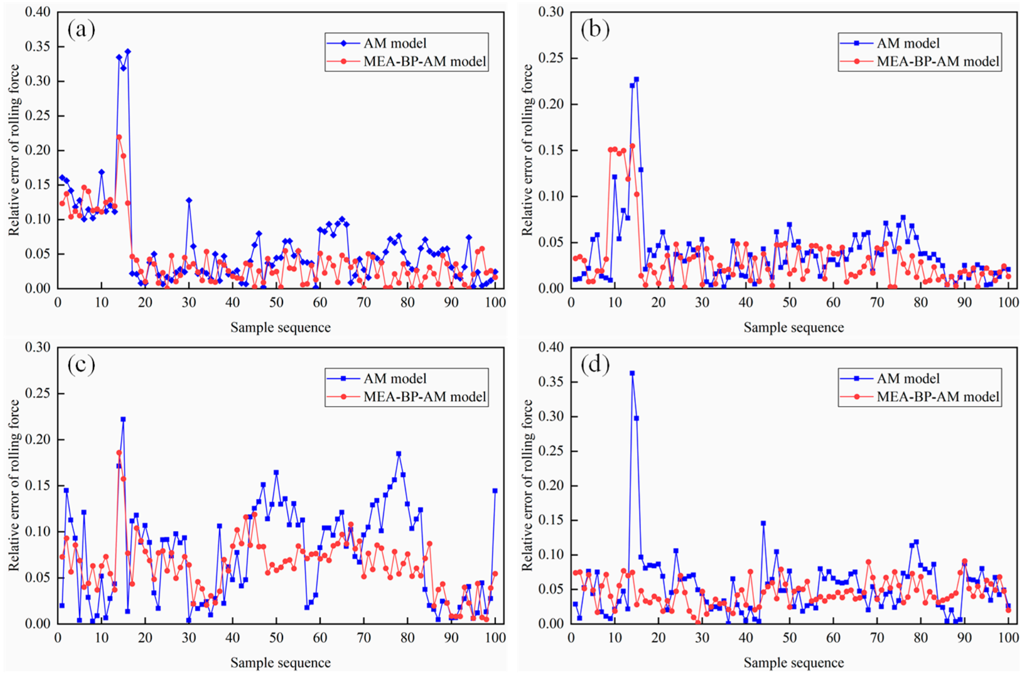

Figure 16. Comparison of rolling force relative error under the AM model and the MEA-BP-AM model. (**a**) Stand 1; (**b**) Stand 2; (**c**) Stand 4; (**d**) Stand 5.

5. Conclusions

This study discussed a novel modeling method predicting deformation resistance for strip cold rolling. The method of obtaining hot and cold rolling data and modeling the combination deformation resistance model is described and verified by testing the model's prediction accuracy.

1. By setting up the "hot-cold rolling" cross-process data platform at the industrial site, the cold rolling and hot rolling processes are unified into an organic whole, which enables online real-time access to the historical production data of hot and cold rolling, and lays a solid data foundation for modeling the deformation resistance of cold rolling based on the hot rolling process data.
2. The back-calculation formula of deformation resistance is derived based on the traditional rolling force model. The measured rolling data of cold rolling is substituted to back-calculate the result of deformation resistance closer to the actual deformation resistance of each stand in the cold rolling process, as the output of the model training and the evaluation criteria of optimization in this paper.
3. A combination model of the analytical model and MEA-BP is established by taking the calculated value of the analytical model directly as an input item of MEA-BP. A small network with the same structure is established for each rack separately so that it learns the hot and cold rolling influencing factors with nonlinear deformation resistance.
4. The prediction accuracies of the analytical model, BP neural network model, and GA-BP neural network model for deformation resistance were near ±12%, ±10%, and ±8%, respectively. The prediction model established by combining the analytical model and MEA-BP reduced the error of deformation resistance calculated for each stand to about ±5%. The comparison results show that combining the analytical model and MEA-BP gives full play to both advantages.
5. Comparing the deformation resistance prediction results of MEA-BP, GA-BP, and BP models, we found that MEA and GA effectively optimize the BP neural network. Still, the unique "similar-taxis" and "dissimilation" operations of MEA can effectively eliminate the problem of new gene defects caused by gene variants in the GA, so the

performance of the MEA-BP neural network is better than GA-BP neural network, and the prediction accuracy of deformation resistance is also higher.

6. The experiment verified the non-negligible influence of the hot rolling process parameters on the cold rolling deformation resistance. The results show that the prediction accuracy of each model for deformation resistance is improved to different degrees when considering the hot rolling parameters as the model input compared to the modeling relying on the single process of cold rolling.
7. In this work, the prediction method proposed by employing both cold and hot rolling data has a more robust prediction capability for cold rolling deformation resistance. More factors, such as the chemical composition, the accelerated cooling parameters after hot rolling and the parameters of thermomechanical hot rolling, may be considered in the following work to further improve the prediction accuracy.

Author Contributions: Conceptualization, methodology, funding acquisition and writing—review and editing, J.Z.; methodology and writing—original draft preparation, J.L.; software and validation H.Q.; validation and funding acquisition, J.S.; resources and investigation, X.W.; supervision and project administration, Q.Y. All authors have read and agreed to the published version of the manuscript.

Funding: This research was funded by the Science and Technology Major Project of Liuzhou City (Grant No. 2021AAD0102) and the China Postdoctoral Science Foundation (Grant No. 2021M690352).

Data Availability Statement: Data sharing not applicable. No new data were created or analyzed in this study. Data sharing is not applicable to this article.

Conflicts of Interest: The funders had no role in the design of the study; in the collection, analyses, or interpretation of data; in the writing of the manuscript; or in the decision to publish the results.

References

1. Paul, S.K.; Ahmed, U.; Megahed, G.M. Effect of hot rolling process on microstructure and properties of low-carbon Al-killed steels produced through TSCR technology. *J. Mater. Eng. Perform.* **2011**, *20*, 1163–1170. [CrossRef]
2. Wang, J.S.; Zhao, Q.L.; Jiao, Z.J.; Liu, X.H. Adaptive learning of the model of deformation resistance model for tandem cold rolling process control. *J. Northeastern. Univ.* **2004**, *25*, 973–976.
3. Guo, L.W.; Yang, Q.; Guo, L. Comprehensive parameters self-adapting for a rolling force model of tandem cold rolling process control. *J. Univ. Sci. Technol. Beijing* **2007**, *29*, 413–416.
4. Bu, H.N.; Ji, X.Y.; Yan, Z.W. Research on online mathematical models of tandem cold Rolling. *IOP Conf. Ser.: Earth Environ. Sci.* **2020**, *512*, 012169. [CrossRef]
5. Liu, H.G.; Tang, D.; Yang, Q.; Guo, L.W. Rolling force prediction model of a multi roll cold tandem mill by fuzzy cerebellum model articulation controller. *J. Univ. Sci. Technol. Beijing* **2006**, *28*, 969–972.
6. Wu, J.G.; Li, Q.; Yan, Y. Emulation and prediction of the cold roll forming force. *Adv. Mater. Res.* **2012**, *206*, 472–475.
7. Lin, J.C. Prediction of rolling force and deformation in three-dimensional cold rolling by using the finite-element method and a neural network. *Int. J. Adv. Manuf. Technol.* **2002**, *20*, 799–806. [CrossRef]
8. Xie, H.B.; Jiang, Z.Y.; Tieu, A.K.; Liu, X.H.; Wang, G.D. Prediction of Rolling Force Using an Adaptive Neural Network Model during Cold Rolling of Thin Strip. *Int. J. Mod. Phys. B* **2014**, *22*, 5723–5727. [CrossRef]
9. Churyumov, A.; Kazakova, A.; Churyumova, T. Modelling of the steel high-temperature deformation behaviour using artificial neural network. *Metals* **2022**, *12*, 447. [CrossRef]
10. Churyumov, A.; Kazakova, A. Prediction of true stress at hot deformation of high manganese steel by artificial neural network Modeling. *Materials* **2023**, *16*, 1083. [CrossRef]
11. Jin, X.; Li, C.S.; Wang, Y.; Li, X.G.; Xiang, Y.G.; Gu, T. Investigation and optimization of load distribution for tandem cold steel strip rolling process. *Metals* **2020**, *10*, 677. [CrossRef]
12. Wu, Z.; Wang, X.; Yang, Q.; Xu, D.; Zhao, J.; Li, J. Deformation resistance prediction of tandem cold rolling based on grey wolf optimization and support vector regression. *J. Iron Steel Res. Int.* **2023**, 1–18. [CrossRef]
13. Zhang, Q.D.; Xu, X.G.; Yu, M.; Qu, B.; Li, S. Cold rolling force model based on GA and ANN for stainless steel strip. *Iron and Steel* **2008**, *43*, 46. [CrossRef]
14. Sun, Y.K.; Zhang, D.Z.; Wang, Y.P.; Cai, H.J. Mended genetic BP network and application to rolling force prediction of 4-stand tandem cold strip mill. *Chin. J. Mech. Eng.* **2004**, *17*, 297–300.
15. Sun, C.Y.; Xie, K.M.; Cheng, M.Q. Mind-evolution-based machine learning framework and new development. *J. Taiyuan Univ. Technol.* **1999**, *30*, 453–457.
16. Wang, F.; Liu, J.; Xie, K.M. Mind evolutionary algorithm design based on group migration. *J. North Univ. China* **2011**, *32*, 303–308.

17. Sun, C.Y.; Sun, Y.; Xie, K.M. Mind-evolution-based machine learning: An efficient approach of evolution computation. In Proceedings of the 3rd World Congress on Intelligent Control and Automation, Hefei, China, 26 June–2 July 2000; Volume 1, pp. 118–121.
18. Jiang, Z.Y.; Wei, D.; Tieu, A.K. Analysis of cold rolling of ultra thin strip. *J. Mater. Process. Technol.* **2009**, *209*, 4584. [CrossRef]
19. Jiang, Z.Y.; Zhu, H.T.; Tieu, A.K. Effect of rolling parameters on cold rolling of thin strip during work roll edge contact. *J. Mater. Process. Technol.* **2003**, *140*, 535. [CrossRef]
20. He, F.; Zhang, L.Y. Mold breakout prediction in slab continuous casting based on combined method of GA-BP neural network and logic rules. *Int. J. Adv. Manuf. Technol.* **2018**, *95*, 4081. [CrossRef]
21. Deng, J.; Gu, D.S.; Li, X.B.; Yue, Z.Q. Structural reliability analysis for implicit performance functions using artificial neural network. *Struct. Saf.* **2005**, *27*, 25. [CrossRef]
22. Mukhopadhyay, A.; Iqbal, A. Prediction of mechanical properties of hot rolled, low-carbon steel strips using artificial neural Network. *Mater. Manuf. Process.* **2005**, *20*, 793. [CrossRef]
23. Liu, H.; Tian, H.Q.; Liang, X.F.; Li, Y.F. New wind speed forecasting approaches using fast ensemble empirical model decomposition, genetic algorithm, mind evolutionary algorithm and artificial neural networks. *Renew. Energ.* **2015**, *83*, 1066. [CrossRef]
24. Wang, J.Z.; Wang, S.T.; Liu, N.; Shang, F.K. A detection method of two carbamate pesticides residues on tomatoes utilizing excitation-emission matrix fluorescence technique. *Microchem. J.* **2021**, *164*, 105920. [CrossRef]
25. Sun, J.; Deng, J.F.; Peng, W.; Zhang, D.H. Strip crown prediction in hot rolling process using random forest. *Int. J. Precis Eng. Man.* **2021**, *22*, 301–311. [CrossRef]